SUPPLEMENTARY INFORMATION FOR

# Structural Effects of Ammonia Binding to the $Mn_4CaO_5$ Cluster of Photosystem II

AUTHORS: David A. Marchiori[1], Paul H. Oyala[1], Richard J. Debus[2], Troy A. Stich[1], and R. David Britt[1,*]

AFFILIATION:

1. Department of Chemistry, University of California, Davis, Davis CA 95616

2. Department of Biochemistry, University of California, Riverside, Riverside CA 92521

E-MAIL: rdbritt@ucdavis.edu

TABLE OF CONTENTS:

**Figure S9.** X-band three-pulse ESEEM of the natural abundance $^{14}$N-ammonia-bound $S_2$-state in the D1-D61A mutant, WT*, and BBY membranes prepared from spinach

**Table S2.** $^{14}$N HFI and NQI Parameters for $NH_3$ Bound to the OEC in the $S_2$ State
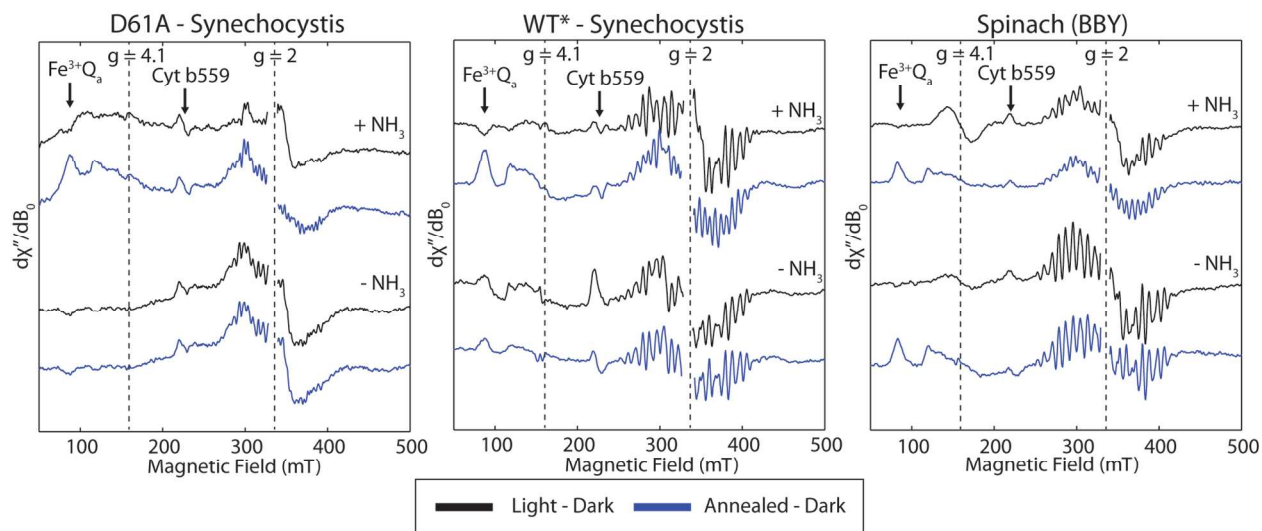
**Figure S1.** Dark subtracted X-band CW EPR of the $S_2$ state of the D1-D61A mutant and WT* from *Synechocystis* and spinach (BBY membranes) in the presence (top traces) and absence (bottom traces) of ammonia. Signals appearing at c.a. 90 mT are assigned to the quinone-ferric iron complex ($Fe^{3+}Q_a$) that is often observed in samples containing PPBQ following low temperature illumination and subsequent annealing. Signals appearing at c.a. 215 mT are assigned to partial oxidation of cytochrome b559 due to the low temperature illumination (170 K) used in these experiments. The field position corresponding to $g = 4.1$ is indicated to show where the high-spin ($S = 5/2$) $S_2$ signal would appear if present, and the field position corresponding to $g = 2$ is also indicated corresponding to the $S = 1/2$ $S_2$ multiline signal. Acquisition parameters: microwave frequency = 9.392 - 9.396 GHz; temperature = 7 K; microwave power = 200 $\mu$W; modulation amplitude = 0.5 mT; conversion time = 82 ms.
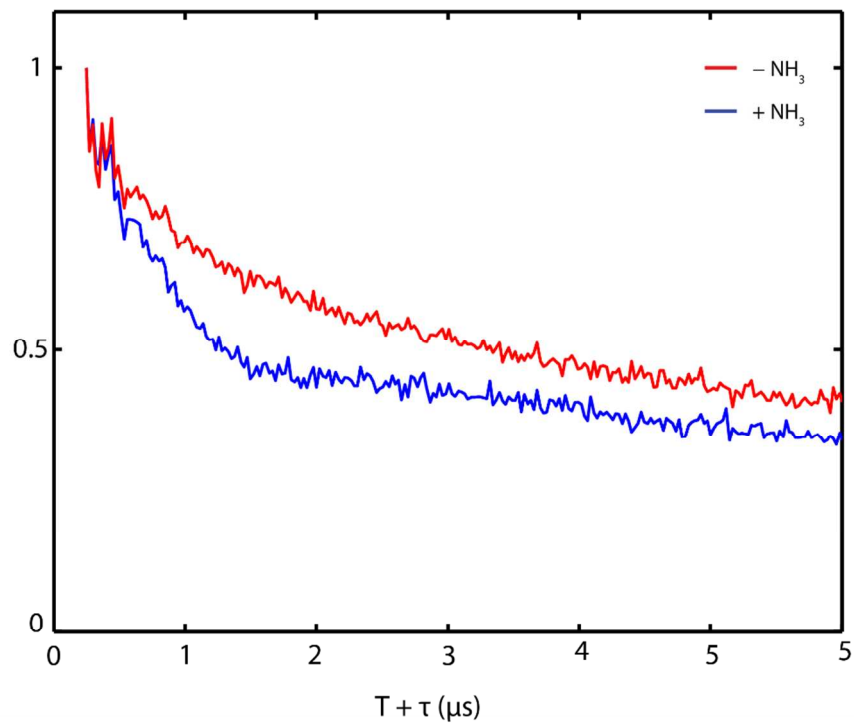
**Figure S2**. X-band 3-pulse ESEEM of the $^{15}$N-ammonia-bound $S_2$-state (blue) and untreated $S_2$-state (red) in BBY membranes prepared from spinach in protiated solvent. Acquisition parameters: microwave frequency = 9.336 GHz; magnetic field = 336.8 mT; temperature = 4.5 K; $\pi/2$ MW pulse length = 12 ns; $T_{init}$ = 40 ns; $\tau$ = 208 ns; rep. time = 5 ms.

The net dipolar contribution of each proton listed in Table S1 was calculated from relevant DFT, QM/MM, and X-Ray structures. Each of the four Mn⋯⋯$^1$H dipolar terms are scaled by the respective spin-projection factors reported in Lohmiller et al.,[1] transformed into a common reference frame, and summed to yield the net dipolar contribution. Simulations were constructed utilizing the salt and saffron routines from the EasySpin toolbox[2-3] for $^1$H ENDOR and $^2$H ESEEM respectively. The $^2$H HFI was computed by scaling the $^1$H HFI by the ratio of the gyromagnetic ratios (i.e. $\gamma_{2H}/\gamma_{1H} \approx 0.154$). Simulations included nuclear quadrupole parameters ($\eta = 0.1$ and $e^2Qq = 0.22$ MHz) for each deuterium nucleus based on previously reported values.[4-5] An isotropic HFI of 2 MHz was included for ligands bound to Mn4A, based on previously reported values.[6] A range of isotropic HFI for O5 ($\pm$ 10 MHz, the width on the $+NH_3$ ENDOR envelope) are shown in Figure S8.
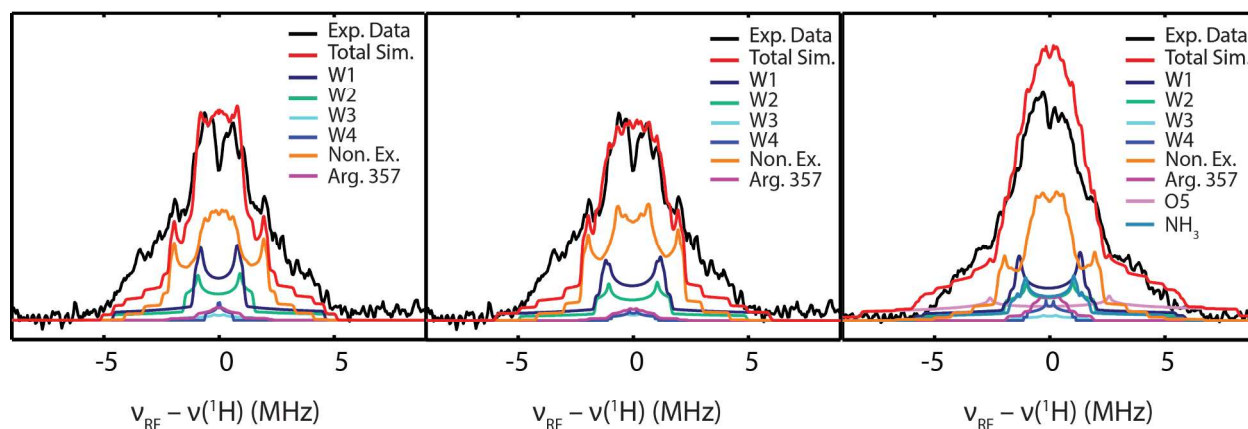


**Figure S3.** Q-band $^1$H Davies ENDOR of the $S_2$ state in absence (left and middle) and presence (right) of ammonia. Left: simulation parameters utilizing coordinates from Shen et al.[7] Middle: simulation parameters utilizing coordinates from Askerka et al.[8] Right: simulation paramters utilizing coordinates from Askerka et al.[9]
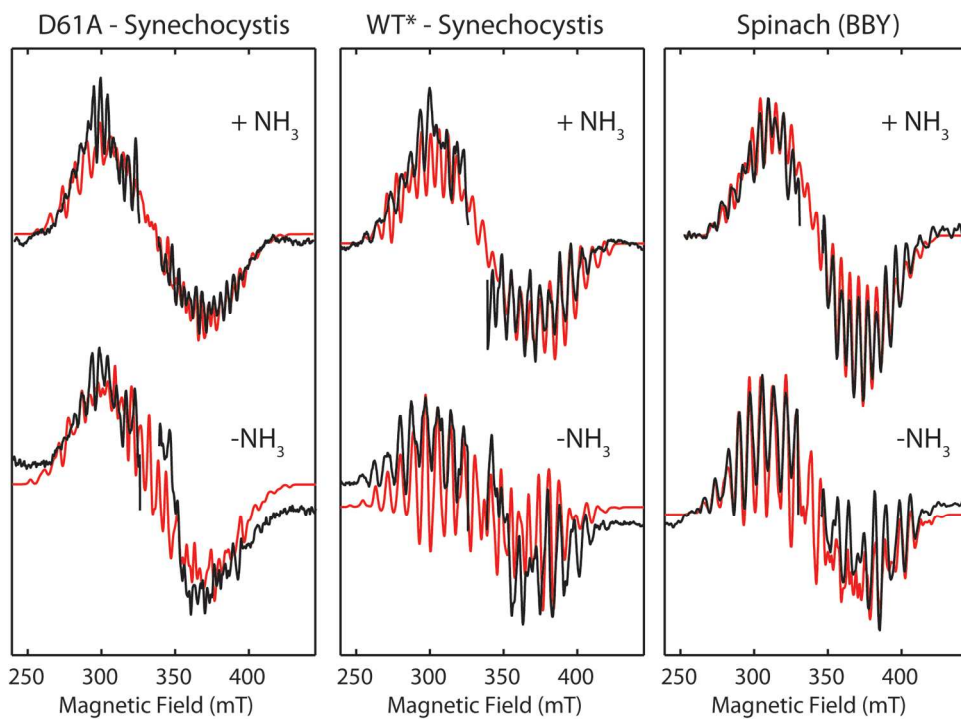
**Figure S4.** X-band CW of the $S_2$ state in the presence (top traces) and absence of ammonia (bottom traces) after annealing at 250 K. Experimental dark-subtracted traces are shown in black, while simulations using the parameters found in Table 2 are shown in red. Acquisition parameters: microwave frequency = 9.39 GHz; temperature = 7 K; MW power = 200 μW; mod. amp. = 5 G; conv. time = 82 ms.

**Figure S5.** Pseudomodulated Q-band [1]H Davies ENDOR of the $S_2$ state in spinach. Black: in the absence of ammonia. Blue: in presence of ammonia after annealing at 250K.

**Table S1.** $A_{dip}$ $^1$H HFI Values (MHz) calculated using multipole point-dipole approximation based on structures from experiment, DFT, and QM/MM. Blue: exchangeable protons. Black: non exchangeable protons.

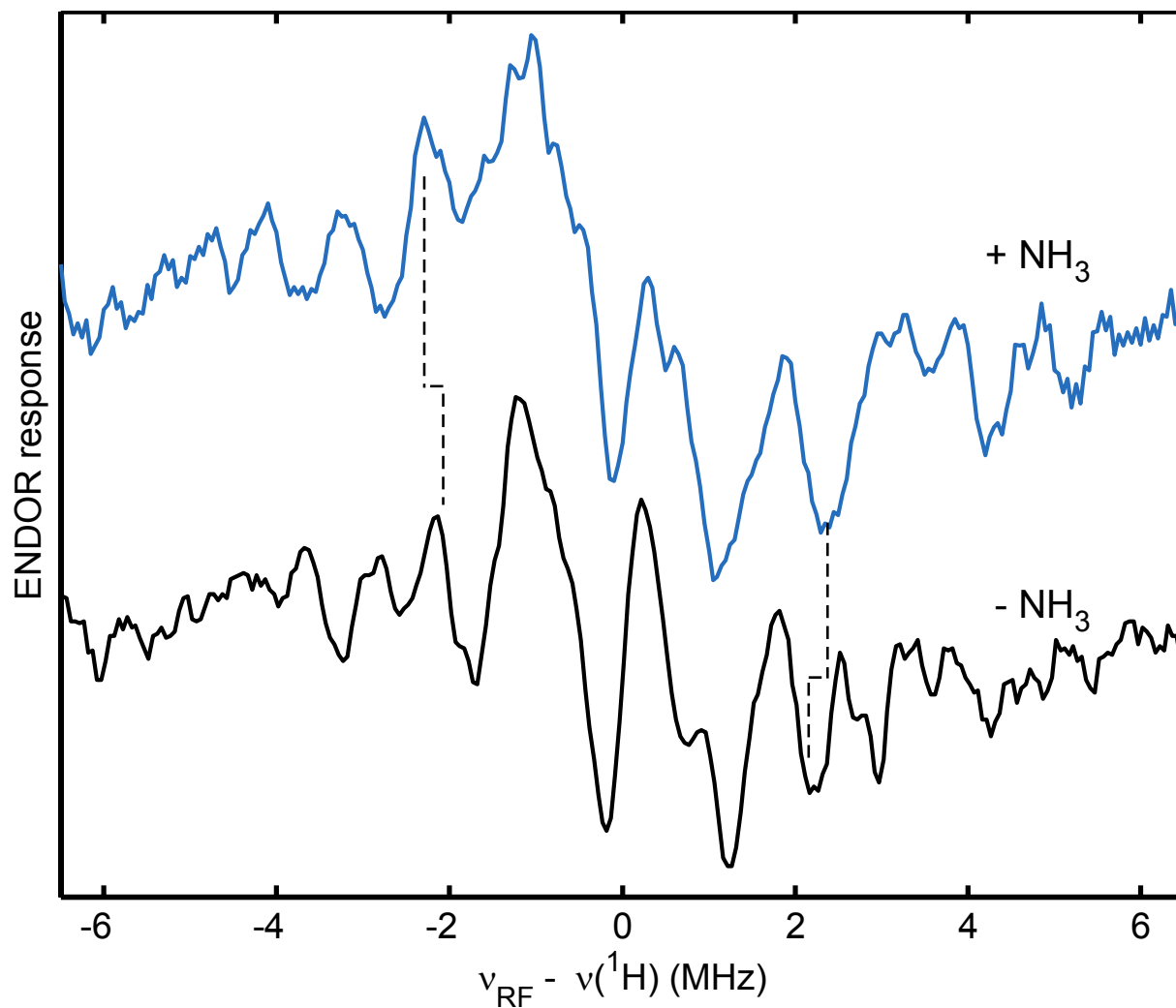| | Lohmiller + NH3 | | | Lohmiller –NH3 | | | Askerka +NH3 | | | Askerka –NH3 | | | Shen –NH3 | | |
|---|---|---|---|---|---|---|---|---|---|---|---|---|---|---|---|
| NH3a | -4.26 | -3.92 | 8.18 | | -- | | -5.32 | -4.57 | 9.89 | | -- | | | -- | |
| NH3b | -4.83 | -3.69 | 8.52 | | -- | | -5.81 | -4.31 | 10.12 | | -- | | | -- | |
| NH3c | -4.52 | -4.11 | 8.62 | | -- | | -4.76 | -4.42 | 9.18 | | -- | | | -- | |
| W1a | | -- | | -4.79 | -3.65 | 8.44 | -4.27 | -3.86 | 8.13 | -5.55 | -4.25 | 9.80 | -4.09 | -3.30 | 7.39 |
| W1b | | -- | | -4.76 | -4.38 | 9.14 | -4.15 | -3.69 | 7.84 | -5.02 | -4.59 | 9.61 | -3.93 | -3.46 | 7.39 |
| W2a | -5.10 | -3.97 | 9.07 | -5.88 | -4.84 | 10.72 | -5.73 | -3.80 | 9.53 | -4.79 | -3.60 | 8.39 | -4.80 | -3.61 | 8.42 |
| W3a | -1.76 | -0.24 | 2.00 | -1.97 | -0.47 | 2.44 | -3.27 | -0.53 | 3.80 | -2.11 | -0.62 | 2.72 | -3.13 | -0.40 | 3.54 |
| W3b | -1.32 | 0.03 | 1.29 | -1.37 | 0.15 | 1.22 | -1.46 | 0.31 | 1.14 | -1.42 | 0.01 | 1.41 | -1.49 | 0.15 | 1.34 |
| W4a | -0.93 | -0.14 | 1.08 | -0.93 | -0.08 | 1.00 | -1.04 | -0.28 | 1.31 | -1.03 | -0.18 | 1.22 | -1.28 | -0.23 | 1.51 |
| W4b | -1.74 | -0.24 | 1.98 | -1.71 | -0.15 | 1.86 | -1.95 | -0.33 | 2.27 | -1.86 | -0.33 | 2.19 | -1.25 | 0.08 | 1.18 |
| His332a | -5.10 | -2.00 | 7.09 | -4.96 | -1.61 | 6.57 | -4.73 | -1.97 | 6.70 | -4.53 | -1.46 | 5.99 | -5.09 | -1.42 | 6.51 |
| His332b | -4.57 | -4.15 | 8.71 | -4.31 | -3.88 | 8.20 | -4.53 | -3.91 | 8.50 | -4.47 | -3.90 | 8.37 | -3.73 | -3.23 | 6.96 |
| His337a | -1.83 | -0.80 | 2.63 | -1.81 | -0.68 | 2.49 | -2.03 | -0.50 | 2.53 | -1.83 | -0.69 | 2.52 | -1.94 | -0.53 | 2.48 |
| His337b | -3.18 | 0.46 | 2.72 | -3.21 | 0.52 | 2.68 | -2.14 | 0.24 | 1.90 | -2.48 | 0.23 | 2.25 | -1.91 | 0.24 | 1.67 |
| CpArg357a | -6.15 | 0.94 | 5.21 | -6.57 | 0.90 | 5.67 | -3.82 | 0.16 | 3.67 | -4.75 | 0.81 | 3.94 | -4.76 | 0.48 | 4.27 |
| CpArg357b | -1.89 | 0.33 | 1.56 | -2.05 | 0.31 | 1.74 | -1.55 | -0.07 | 1.62 | -2.11 | 0.65 | 1.45 | -1.91 | 0.51 | 1.40 |
| CpArg357c | -2.77 | 0.75 | 2.02 | -2.63 | 0.60 | 2.03 | -2.31 | 0.71 | 1.60 | -2.19 | 0.26 | 1.93 | -2.09 | 0.20 | 1.90 |
| CpArg357d | -1.37 | 0.49 | 0.88 | -1.33 | 0.45 | 0.89 | -0.79 | 0.21 | 0.59 | -0.72 | 0.20 | 0.51 | -0.75 | 0.21 | 0.54 |
| Ala344 | -1.02 | 0.29 | 0.73 | -1.03 | 0.33 | 0.70 | | -- | | | -- | | -1.07 | 0.26 | 0.81 |
| Glu333a | -1.34 | 0.18 | 1.16 | -1.44 | 0.18 | 1.26 | | -- | | -1.41 | -0.26 | 1.68 | -1.26 | -0.17 | 1.43 |
| Glu333b | -1.22 | -0.13 | 1.34 | -1.34 | -0.21 | 1.55 | | -- | | -1.57 | -0.01 | 1.58 | -1.38 | 0.21 | 1.17 |
| Glu189a | -1.27 | -1.05 | 2.32 | -1.20 | -0.96 | 2.16 | -1.37 | -1.19 | 2.56 | -1.45 | -1.24 | 2.70 | -1.36 | -1.16 | 2.51 |
| Glu189b | -1.79 | -1.61 | 3.40 | -1.68 | -1.49 | 3.17 | -1.84 | -1.58 | 3.42 | -2.01 | -1.67 | 3.68 | -1.74 | -1.51 | 3.24 |

| | | | | | | | | | | | | | | | |
|---|---|---|---|---|---|---|---|---|---|---|---|---|---|---|---|
| Asp170 | -1.24 | -0.98 | 2.21 | -1.43 | -1.18 | 2.61 | -1.18 | -0.96 | 2.14 | -1.49 | -1.22 | 2.71 | -1.48 | -1.24 | 2.73 |
| O5 | -- | | | -- | | | -16.40 | -5.17 | 21.57 | -- | | | -- | | |
| WA5A | -2.50 | -1.70 | 4.21 | -2.68 | -2.33 | 5.01 | -1.10 | -0.77 | 1.87 | -0.90 | -0.66 | 1.56 | -1.13 | -0.78 | 1.91 |
| WA5B | -0.90 | -0.56 | 1.46 | -1.26 | -0.89 | 2.15 | -0.82 | -0.67 | 1.49 | -0.89 | -0.67 | 1.56 | -1.73 | -1.47 | 3.20 |
| WA2A | -5.90 | 0.73 | 5.17 | -6.51 | 0.67 | 5.83 | -1.51 | -0.77 | 2.28 | -5.15 | -2.36 | 7.51 | -5.06 | -1.07 | 6.13 |
| WA2B | -1.70 | -0.24 | 1.93 | -1.92 | -0.34 | 2.26 | -1.68 | -0.26 | 1.94 | -1.37 | -0.39 | 1.76 | -2.10 | 0.11 | 1.99 |
| WA1A | -3.00 | 1.44 | 1.56 | -2.68 | -2.33 | 5.01 | -0.96 | -0.18 | 1.15 | -2.59 | -2.06 | 4.65 | -1.15 | -0.50 | 1.65 |
| WA1B | -1.83 | 0.58 | 1.25 | -1.26 | -0.89 | 2.15 | -1.72 | -1.03 | 2.75 | -1.20 | -0.70 | 1.90 | -1.55 | -1.09 | 2.64 |
| WA3A | -1.28 | -0.60 | 1.88 | -1.64 | -0.61 | 2.25 | -1.59 | -1.09 | 2.69 | -1.24 | -0.92 | 2.16 | -0.79 | -0.40 | 1.19 |
| WA3B | -0.63 | -0.23 | 0.86 | -1.64 | -1.16 | 2.80 | -0.78 | -0.34 | 1.11 | -0.75 | -0.45 | 1.20 | -0.82 | -0.54 | 1.36 |
| Wb1A | -0.60 | -0.19 | 0.79 | -3.27 | 1.52 | 1.75 | -2.28 | 0.66 | 1.63 | -4.52 | 1.35 | 3.18 | -3.25 | 1.30 | 1.95 |
| Wb1B | -0.67 | -0.22 | 0.88 | -2.02 | 0.57 | 1.45 | -0.77 | 0.14 | 0.63 | -1.21 | 0.27 | 0.94 | -0.95 | 0.30 | 0.66 |
| WD1A | -2.57 | -0.22 | 2.78 | -2.52 | -0.14 | 2.65 | -7.88 | -1.03 | 8.90 | -3.02 | -0.21 | 3.23 | -4.34 | -3.77 | 8.11 |
| WD1B | -8.52 | -1.25 | 9.77 | -8.32 | -0.99 | 9.31 | -2.07 | -0.65 | 2.71 | -1.81 | -0.82 | 2.63 | -2.89 | -2.78 | 5.66 |
| WCa1A | -1.00 | -0.65 | 1.65 | -1.25 | -0.49 | 1.74 | -1.17 | -0.52 | 1.69 | -0.74 | -0.15 | 0.89 | -1.17 | -0.48 | 1.65 |
| WCa1B | -0.60 | -0.46 | 1.06 | -0.62 | -0.18 | 0.80 | -0.63 | -0.18 | 0.80 | -0.47 | -0.21 | 0.68 | -0.61 | -0.21 | 0.82 |
| WCa2A | -1.73 | -0.54 | 2.26 | -0.62 | -0.16 | 0.79 | -1.59 | -1.09 | 2.69 | -0.50 | -0.24 | 0.74 | -0.55 | -0.21 | 0.75 |
| WCa2B | -1.47 | -0.97 | 2.44 | -0.73 | -0.25 | 0.98 | -0.78 | -0.34 | 1.11 | -0.32 | -0.17 | 0.48 | -0.37 | -0.33 | 0.70 |
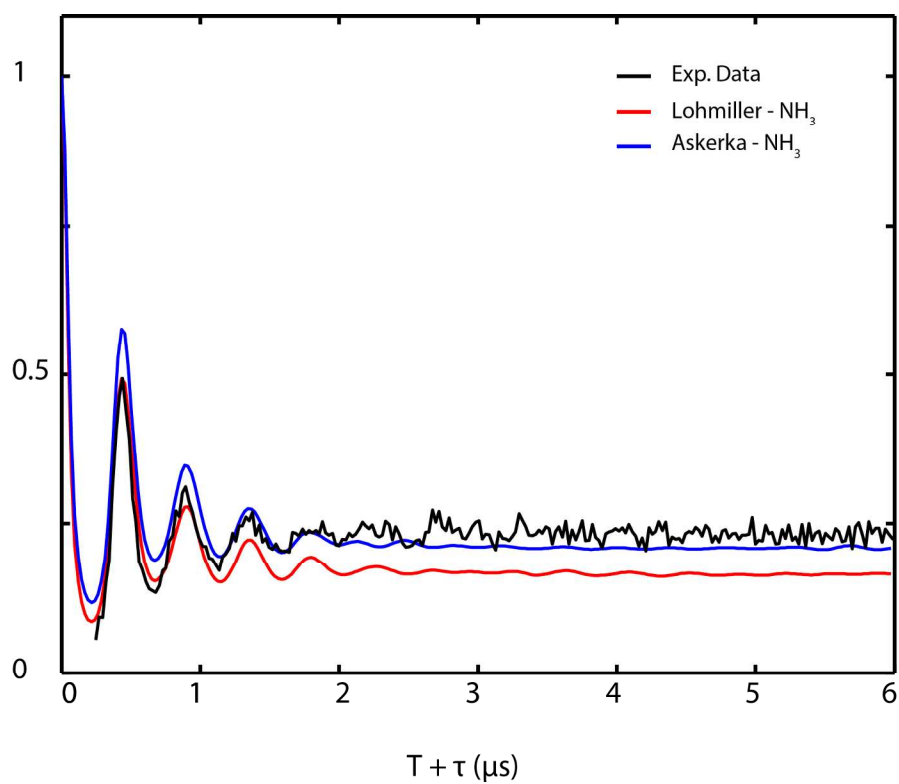
**Figure S6.** X-band 3-pulse ESEEM of the untreated $S_2$-state (black) with DFT and QM/MM based simulations (colored).
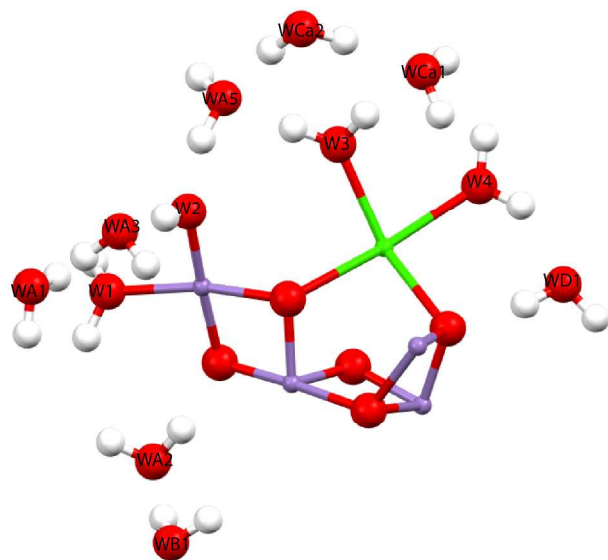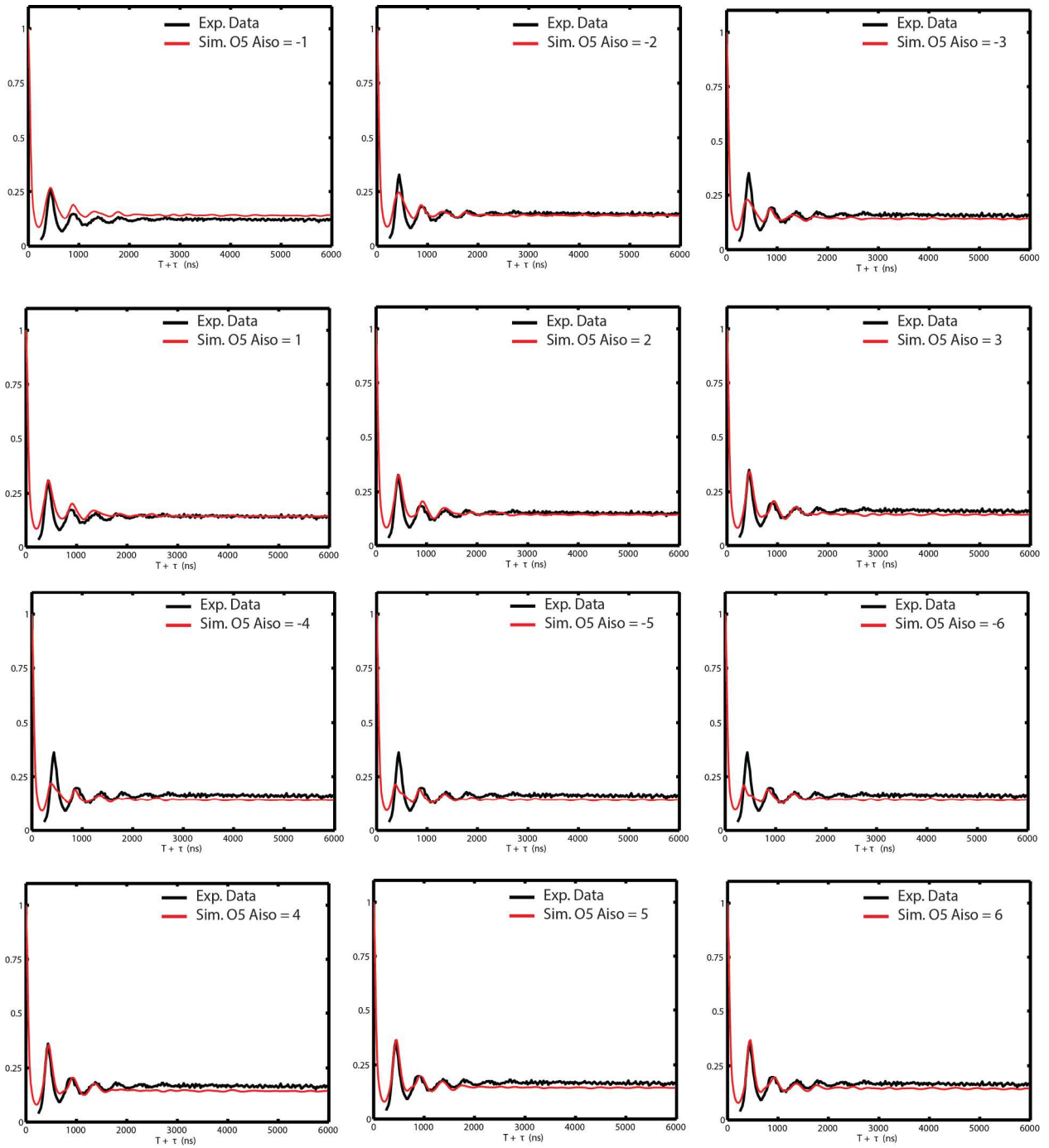
**Figure S7.** Model from Lohmiller et al. depicting waters within ~5 Å of the OEC.
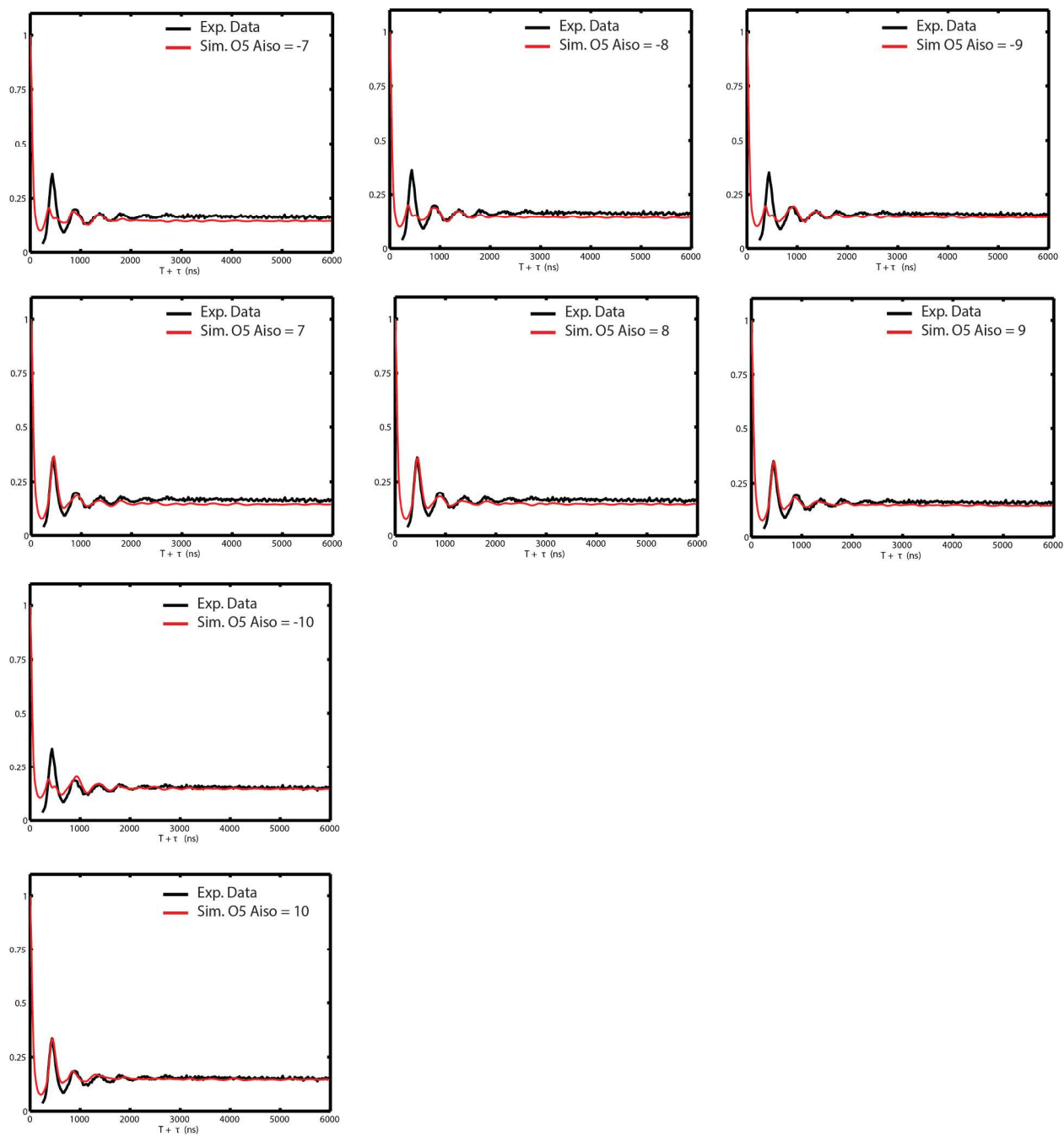
**Figure S8.** X-band 3-Pulse ESEEM simulations of the "Carousel" model of Askerka et al. using Aiso values of ± 10 MHz. $^{1}$H Aiso values shown in figure captions are multiplied by gyromagnetic ratios for $^{2}$H and $^{1}$H (i.e. $\gamma_{2H}/\gamma_{1H} \approx 0.154$) to yield the resultant 3-Pulse ESEEM simulations.

The magnetic parameters of the ammonia nitrogen bound to the OEC (Table S2) were determined by simulation of the corresponding X-band ESEEM spectra (Figure S9). In our re-evaluation of the coupling constants determined for ammonia bound to spinach PSII, we achieved a better fit of the data by decreasing the electric field asymmetry parameter $\eta$ from $0.59^{10}$ to 0.402 and by adding significant rhombicity to the $^{14}$N hyperfine anisotropy (cf. $A_{aniso}$ = [−0.20, −0.20, +0.40] MHz determined previously[10] to $A_{aniso}$ = [−0.37, +0.44, −0.07] MHz from the present work). This change brings the value for $\eta$ more in line with those determined for ammonia-treated PSII from *T. elongatus* ($\eta$ = 0.47)[11] and *Synechocystis* ($\eta$ = 0.40)[12], indicating that the ammonia nitrogen nucleus experiences a similar electrostatic environment in PSII from all three organisms. In particular, the $^{14}$N ESEEM spectra for $NH_3$ bound to the $S_2$ state in PSII from spinach were indistinguishable from those obtained for WT* PSII from *Synechocystis* (see Figure S9 and corresponding simulation parameters in Table S2).

As we reported previously,[12] mutation of D1-Asp61 to alanine in *Synechocystis* collapses the electric field asymmetry parameter ($\eta$ = 0.042) as one would expect for a $C_{3v}$-symmetric terminal ammonia ligand. Thus we concluded that the large asymmetry observed for native PSII preparations results from a strong hydrogen bond between the carboxylate of Asp61 and one of the ammonia protons. As the X-ray structures of PSII from *Thermosynechococcus vulcanus* show Asp61 as forming a hydrogen bond with W1 bound to Mn4A (Figure 1A),[7] we concluded that ammonia must be binding in place of W1. Given the similar $^{14}$N-ammonia HFI and NQI parameters (Table S2), the interaction between $NH_3$, Mn4A, and Asp61 in the ammonia-bound $S_2$ state is likely identical in PSII from all three organisms.
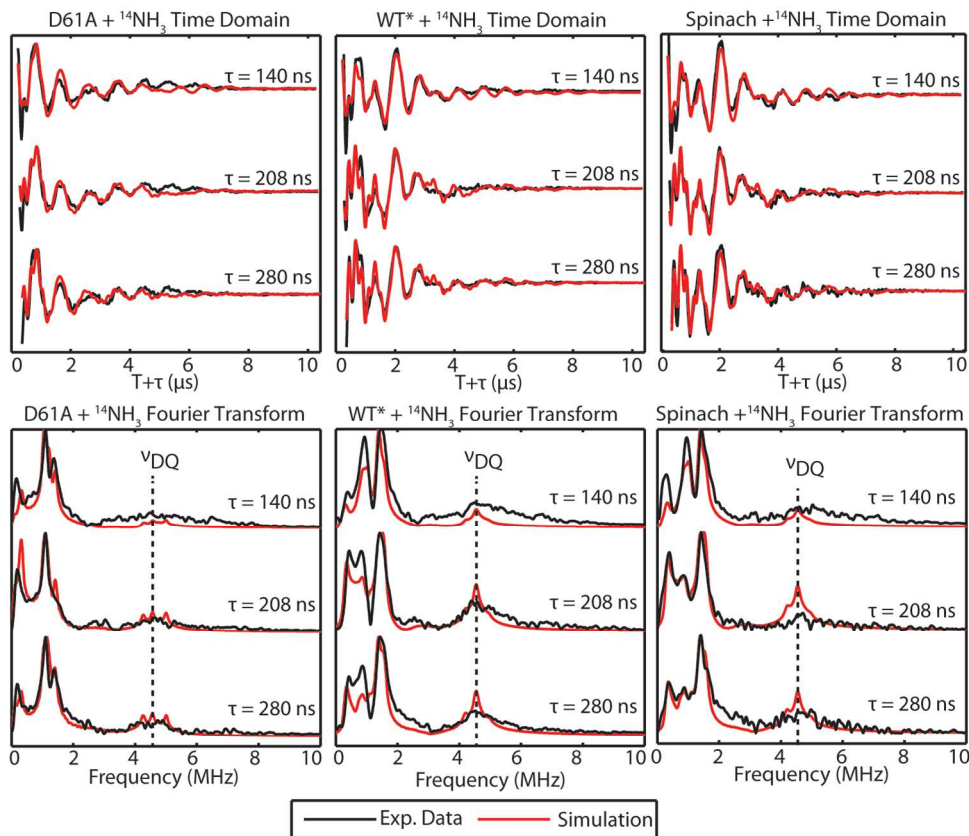
**Figure S9.** X-band three-pulse ESEEM of the natural abundance $^{14}$N-ammonia-bound $S_2$-state in the D1-D61A mutant (left-hand panels), WT* (center panels) and BBY membranes prepared from spinach (right-hand panels). For each, the top panel shows the time-domain data after subtraction of a biexponential decay function, and the bottom panel displays the Fourier transform of each time trace using cross-term averaging. Black traces represent the experimental data, while red traces represent the simulated spectrum using the simulation parameters in Table 3. Acquisition parameters: microwave frequency = 9.319 GHz (D1-D61A), 9.329 GHz (WT*), 9.313 GHz (Spinach); magnetic field = 335.5 mT (D1-D61A), 336.4 mT (WT*), 336.0 mT (Spinach); temperature = 4.5 K; $\pi/2$ MW pulse length = 12 ns; repetition time = 5 ms.

**Table S2.** $^{14}$N HFI and NQI Parameters for NH$_3$ Bound to the OEC in the $S_2$ State.

| Species | $A_{iso}$ (MHz) | $A_{x,y,z}$ (MHz) | $e^2qQ/\hbar$ (MHz) | $\eta$ | A and P Euler angles $(\alpha,\beta,\gamma)°$ | Ref. |
|---|---|---|---|---|---|---|
| Spinach | 2.33 | [1.96 2.76 2.26] | 1.616 | 0.402 | (5, 98 110) | This work |
| Spinach | 2.29 | [2.09 2.09 2.69] | 1.61 | 0.59 | (0, 0, 0) | 10 |
| WT* *Synechocystis* | 2.33 | [1.96 2.76 2.26] | 1.616 | 0.402 | (5, 98 110) | 12 |
| *T. elongatus* | 2.36 | [2.77 2.62 1.69] | 1.52 | 0.47 | Not reported | 11 |
| D61A *Synechocystis* | 2.36 | [1.98 2.78 2.31] | 1.536 | 0.042 | (13, 51, 148) | 12 |

**References**

1.      Lohmiller, T.; Krewald, V.; Navarro, M. P.; Retegan, M.; Rapatskiy, L.; Nowaczyk, M. M.; Boussac, A.; Neese, F.; Lubitz, W.; Pantazis, D. A. et al, Structure, ligands and substrate coordination of the oxygen-evolving complex of photosystem II in the S2 state: a combined EPR and DFT study. *Phys. Chem. Chem. Phys.* **2014,** *16*, 11877-11892.

2.      Stoll, S.; Schweiger, A., EasySpin, a comprehensive software package for spectral simulation and analysis in EPR. *J. Magn. Reson.* **2006,** *178*, 42-55.

3.      Stoll, S.; Britt, R. D., General and efficient simulation of pulse EPR spectra. *Phys. Chem. Chem. Phys.* **2009,** *11*, 6614 - 6625.

4.      Randall, D. W.; Gelasco, A.; Caudle, M. T.; Pecoraro, V. L.; Britt, R. D., ESE-ENDOR and ESEEM Characterization of Water and Methanol Ligation to a Dinuclear Mn(III)Mn(IV) Complex. *J. Am. Chem. Soc.* **1997,** *119*, 4481-4491.

5.      Force, D. A.; Randall, D. W.; Lorigan, G. A.; Clemens, K. L.; Britt, R. D., ESEEM Studies of Alcohol Binding to the Manganese Cluster of the Oxygen Evolving Complex of Photosystem II. *J. Am. Chem. Soc.* **1998,** *120*, 13321-13333.

6.      Aznar, C. P.; Britt, R. D., Simulations of the 1H electron spin echo-electron nuclear double resonance and 2H electron spin echo envelope modulation spectra of exchangeable hydrogen nuclei coupled to the S2-state photosystem II manganese cluster. *Philos. Trans. R. Soc. London, Ser. B* **2002,** *357*, 1359-1366.

7.      Suga, M.; Akita, F.; Hirata, K.; Ueno, G.; Murakami, H.; Nakajima, Y.; Shimizu, T.; Yamashita, K.; Yamamoto, M.; Ago, H. et al, Native structure of photosystem II at 1.95 angstrom resolution viewed by femtosecond X-ray pulses. *Nature* **2015,** *517*, 99-103.

8.      Askerka, M.; Wang, J.; Brudvig, G. W.; Batista, V. S., Structural Changes in the Oxygen-Evolving Complex of Photosystem II Induced by the S-1 to S-2 Transition: A Combined XRD and QM/MM Study. *Biochemistry* **2014,** *53*, 6860-6862.

9.      Askerka, M.; Vinyard, D. J.; Brudvig, G. W.; Batista, V. S., NH3 Binding to the S-2 State of the O-2-Evolving Complex of Photosystem II: Analogue to H2O Binding during the S-2 -> S-3 Transition. *Biochemistry* **2015,** *54*, 5783-5786.

10.     Britt, R. D.; Zimmermann, J. L.; Sauer, K.; Klein, M. P., Ammonia binds to the catalytic manganese of the oxygen-evolving complex of photosystem II. Evidence by electron spin-echo envelope modulation spectroscopy. *J. Am. Chem. Soc.* **1989,** *111*, 3522-3532.

11.     Perez Navarro, M.; Ames, W. M.; Nilsson, H.; Lohmiller, T.; Pantazis, D. A.; Rapatskiy, L.; Nowaczyk, M. M.; Neese, F.; Boussac, A.; Messinger, J. et al, Ammonia binding to the oxygen-evolving complex of photosystem II identifies the solvent-exchangeable oxygen bridge (mu-oxo) of the manganese tetramer. *Proc. Natl. Acad. Sci. U.S.A.* **2013,** *110*, 15561-15566.

12.     Oyala, P. H.; Stich, T. A.; Debus, R. J.; Britt, R. D., Ammonia Binds to the Dangler Manganese of the Photosystem II Oxygen-Evolving Complex. *J. Am. Chem. Soc.* **2015,** *137*, 8829-8837.